

Two-Dimensional Aerodynamic Analysis of Multiple-Elements Airfoils Using Computational Fluid Dynamics (CFD) Software

Fakhrul Fahmi Zamzuri¹, Zurriati Mohd Ali^{-1,*}, Ahmad Fathi Azad¹, Nor Afifah Yahaya¹ and Iskandar Shah Ishak² ¹Faculty of Mechanical Engineering, Universiti Teknologi MARA, Shah Alam 40450 Selangor, Malaysia. ²UTM Aerolab, Institute for Sustainable Transport, Universiti Teknologi Malaysia, 81310 UTM Johor Bahru, Johor, Malaysia *corresponding author: zurriatimohdali@uitm.edu.my

ABSTRACT

Multiple-element airfoils consist of two or more airfoil sections positioned closely together, and they are commonly used to enhance lift during takeoff and landing. These configurations can be found in aircraft wings and wind turbines because of their ability to generate greater lift and improve aerodynamic performance. However, optimizing their arrangement can be challenging, as suboptimal configurations may lead to increased drag. This study examines three multiple-airfoil configurations: (A) NACA 2412–NACA 0012, (B) NACA 2412–NACA 2415, and (C) NACA 2412–Clark Y. Computational fluid dynamics (CFD) simulations were conducted using ANSYS Fluent with the Spalart–Allmaras turbulence model at a Reynolds number (Re) of 1.34×10^6 and a velocity (V) of 20 m/s. The lift and drag characteristics were analysed for angles of attack (α) ranging from 0° to 19°. The results indicate that all configurations exhibit similar trends in lift and drag; however, Set C demonstrates a delay in stall, while Sets A and B achieve the highest lift-to-drag ratio (approximately 32) at an angle of 5°. These findings enhance our understanding of the performance of multi-element airfoils and their role in improving aerodynamic efficiency during takeoff.

Keywords: Computational Fluid Dynamics; NACA 2412; Multiple- Airfoil; Lift coefficient; Drag coefficient

Nomenclature

 $\begin{array}{ll} l & \text{Airfoil lift} \\ d & \text{Airfoil Drag} \\ \alpha & \text{Angle of attack} \\ \textit{Re} & \text{Reynolds Number} \end{array}$

V Velocity

Abbreviations

L/D Lift-to-drag ratio

1.0 INTRODUCTION

In aviation, takeoff refers to the moment when an aircraft lifts off the ground and begins its flight. During takeoff, the aircraft operates at a lower speed in the takeoff roll compared to its cruising speed because it is still accelerating and has not yet reached the necessary speed for sustained flight. At these lower speeds, multiple-element wings, such as slotted flaps and slats, significantly increase the aerodynamic lift by enhancing the camber and effective surface area of the wings [1]. This capability enables the aircraft to take off at a lower speed, thereby reducing the required length of the takeoff roll. The increased lift at lower speeds results in a steeper climb angle, facilitating clearance over obstacles during takeoff.

For multiple-element wings, an aircraft uses different types of flaps to enhance lift and improve stall characteristics by controlling the airflow and maximizing the aerodynamic efficiency. According to Kluga [2], the size of the flaps typically ranges from 15% to 25% of the main wing chord. The common designs of flaps used in multi-element wings include plain, split, slotted, and Fowler types. Figure 1 shows the types of flaps and their effect on the lift force of the wing.

The graph demonstrates that adding the flap significantly increases the maximum lift. Additionally, the zero-lift angle of attack shifts to a greater negative value, and there is an increase in drag. Using a flap can create a twisting moment that causes the nose to tilt downward, and the Fowler flaps typically generate the greatest twisting

moment. A plain airfoil is a simple hinged component located at the back of the wing that tilts downward to enhance lift; however, this can also cause the nose of the plane to dip. In contrast, a split airfoil lowers only the bottom portion of the wing's trailing edge. Although this design significantly increases drag, which aids in steep landings, it also causes the nose to drop. A more effective alternative is the slotted airfoil, which features a small gap between the flap and the wing [4]. This gap allows air to flow through, improving the wing's efficiency and increasing lift.

Flaps utilize specific airfoil sections designed to optimize lift, drag, and stall characteristics. Common types of airfoil sections used for flaps include symmetrical airfoils, cambered airfoils, NACA 4-digit series, NACA 5digit series, supercritical airfoils, high-lift airfoils, and multi-element airfoils. Airfoil section properties differ from those of the wing or airplane due to the effects of the planform. The properties of the airfoil are derived from its basic shape or profile in 2D flow. The selection of suitable airfoils and configuration is a critical step in aerodynamic analysis. Various factors, including the airfoil's shape, camber, thickness, and angle of attack, significantly influence its performance. Choosing the appropriate airfoil for a specific application often involves a trade-off between high lift coefficients, minimal drag, and structural feasibility. Research has shown that aircraft with multi-element airfoils can significantly enhance flight performance. For instance, Hariyadi et al. [5] studied a NACA 43018 design featuring a slat and a slotted flap, which found that this setup improves the lift-to-drag ratio at higher angles of attack, though it may be less effective at lower ones. In another study, Esabat et al.[6] explored a wavy (corrugated) airfoil identified as W1011. Their findings revealed a substantial increase in lift coefficient at larger flap angles and a notable enhancement in lift-to-drag ratio, particularly at lower angles of attack. These insights strongly advocate for the adoption of wavy airfoils in future aircraft designs. In this study, slotted airfoils were selected for investigation. The choice of a 15% chord gap and a second airfoil deflection angle of 20 degrees is supported by the findings of Velkova and Todorov[7], which emphasized the importance of optimizing the gap size between the wing and the slotted flap to improve aerodynamic efficiency. The study demonstrated that the proper sizing of the gap and flap deflection has a significant impact on lift and drag characteristics, especially for ultra-light aircraft configurations.

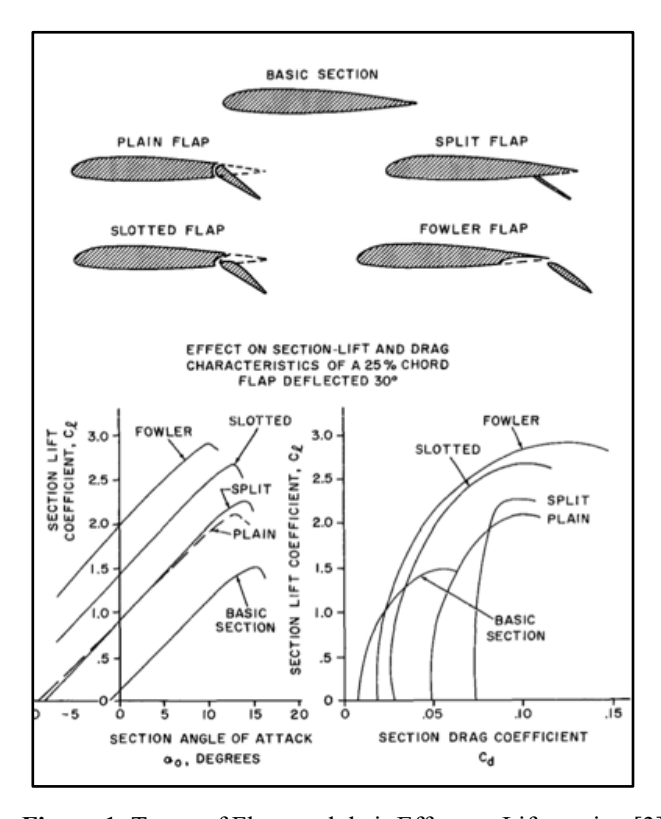


Figure 1: Types of Flaps and their Effect on Lift-section [3]

This study utilized computational fluid dynamics (CFD) to simulate the flow around multi-airfoil configurations. CFD is essential for researching and designing airfoils, as it provides detailed insights into their aerodynamic properties. It offers a cost-effective and precise method for analysing airfoil performance compared to traditional wind tunnel tests. Additionally, CFD allows for the simulation of various flight conditions and design variations without the need for physical prototypes. CFD effectively models complex flow phenomena, such as turbulence and flow separation, which are challenging to capture through experimental methods [8]. Typically, the Reynolds-Averaged Navier-Stokes (RANS) equations are employed to accurately model turbulence, with advanced models like k-ε and k-ω enhancing the precision of these simulations. Research has indicated that CFD accurately predicts lift and drag characteristics, which are crucial for assessing aerodynamic efficiency [9]. For instance, CFD analyses of NACA airfoils have demonstrated good agreement with experimental data, confirming the reliability of CFD. Furthermore, parametric studies using CFD enable systematic variations of design parameters, allowing for an assessment of their impact on performance [10].

Turbulence modeling is a fundamental aspect of Computational Fluid Dynamics (CFD) used to predict the behaviour of fluid flow. Accurate turbulence modeling is crucial for simulating complex flows in various engineering applications, such as aerospace, automotive, and environmental engineering. The Spalart-Allmaras model is a one-equation turbulence model that has been developed primarily for aerodynamic flows [11]. Moreover Spalart-Allmaras model is the fastest as compared to others [12]. From the day of its introduction in 1992, this model is found to have more application in the field of aerodynamics in solving problems with turbulent flow. This method is considered to be the most efficient and effective model for conducting the aerodynamic flow analysis in structures such as airfoils, wings, fuselages, missiles and ship hulls by the simulation community as it takes lesser time, iterations and cost to provide results of higher accuracy [13].

Research has focused on individual airfoils, but few studies have compared how they perform together in multi-element configurations. For example, the NACA 2412 is a moderately cambered airfoil often used in general aviation. It has good lift characteristics and behaves smoothly when stalling. The NACA 0012 is symmetrical and offers neutral pitching moments, making it a suitable secondary element to help delay flow separation. The NACA 2415 has more camber and thickness than the NACA 2412, giving it higher lift but also causing more drag at larger angles of attack. The Clark Y airfoil has a nearly flat lower surface, which makes it easy to build and stable at low speeds, making it popular for light aircraft. Even though each airfoil has strengths, there is little analysis of how they work together in multi-element configurations, especially during low-speed takeoff. This study aims to find out how different flap profiles affect lift, drag, and stall characteristics in these multi-airfoil designs using Computational Fluid Dynamics (CFD) simulation.

2.0 METHODOLOGY

2.1 Computational model

The fluid flow around the multi-element airfoil is simulated using the computational fluid dynamics software, Ansys Fluent. The purpose of this simulation is to determine the lift and drag coefficients for this configuration, as well as to visualize the flow around it. The process began by constructing the model using data from the Airfoil Tool [14], which was later be imported into Ansys Fluent for further simulation. In the pre-processing phase, the computational model was constructed based on research conducted by Velvoka and Todorov [7]. However, the airfoil profile was updated to include the NACA 2412 as the main wing, with the NACA 0012 (symmetrical airfoil), NACA 2145 (cambered airfoil), and Clark Y (cambered airfoil with flat lower surface from 30% chord to the trailing edge) airfoils serving as flaps, as shown in Figure 2. In this study, slotted airfoils were selected for investigation. The choice included a 15% chord gap and a second airfoil deflection angle of 20 degrees. The arrangement of the main airfoil with a flap was divided into three sets to facilitate discussion of the results.

Table 1 shows the arrangement of these multi-element airfoils. In the infinite wing (2D) model, there is no wingtip effect. For a given airfoil shape, the lift and drag force of the aircraft depends on several factors, including the incoming velocity (V), air density (ρ), wing area (S), viscosity coefficient (μ), and the speed of sound (a). These parameters can be summarized into a lift and drag coefficient, which is calculated by dividing the aerodynamic forces (lift, L, and drag, D) with the dynamic pressure multiplied by a reference area. For wings, the most convenient reference area is denoted as S. The formula for the lift and drag coefficient (C_1) is as follows:

$$C_L = \frac{L}{1/2\rho V^2 S} \qquad (1)$$

$$C_D = \frac{D}{1/2\rho V^2 S} \qquad (2)$$

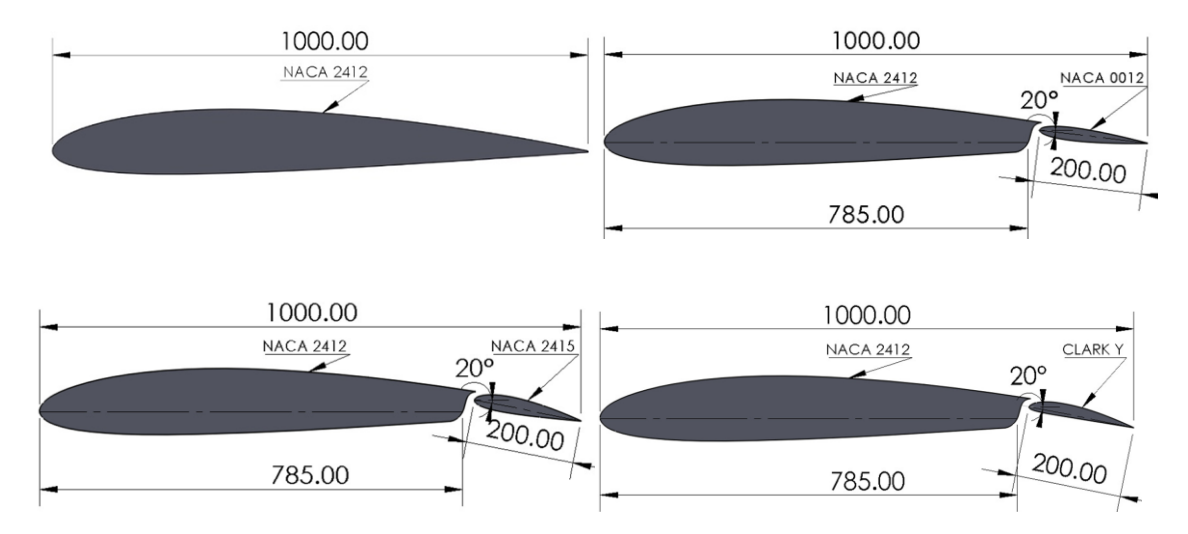


Figure 2: Multiple-airfoil Arrangement with different Flap Airfoil Profile (in mm)

Set	Arrangement	
Default	NACA 2412	
A	NACA 2412 and NACA 0012	
В	NACA 2412 and NACA 2415	
С	NACA 2412 and Clark-Y	

 Table 1: Airfoil Arrangement

2.2 Computational set-up (pre-processing)

Figure 3(a) illustrates the computational domain and mesh surrounding the airfoil. A C-type computational domain was established to simulate the airflow around the airfoil. The inlet was positioned 10 chord lengths (10c) upstream of the airfoil to minimize the influence of inlet pressure, while the outlet was located 15 chord lengths (15c) downstream to effectively capture wake formation and pressure recovery. Mesh generation is a critical aspect of this research, as high-quality meshing leads to improved results. In this study, a structured mesh was employed due to the complexity of the model, as shown in Figure 3(b). Although this type of mesh allows for flexible handling of geometry, it is also more computationally expensive. The entire volume mesh was composed of 132537 elements and 133197 nodes.

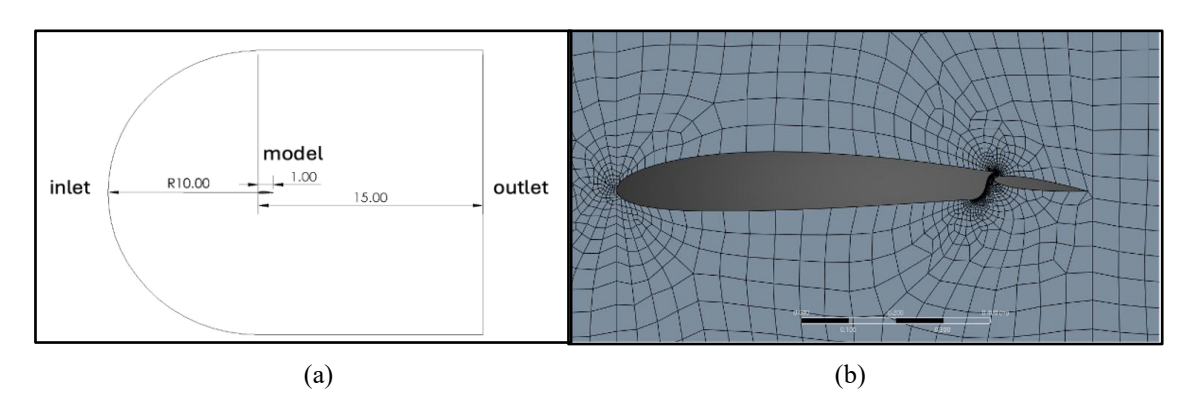


Figure 3: (a) Computational Model; (b) Model meshing

The study focused on the Reynolds-Averaged Navier-Stokes (RANS) equation applied to the flow domain over a multielement airfoil. For this analysis, the Spalart-Allmaras turbulence model was chosen due to its efficiency and suitability for external aerodynamic flows. The boundaries surrounding the model surfaces were defined as a far field, with a free-stream velocity set at 20 m/s. The Reynolds number (Re) based on the model chord was 1.34×10^6 , while the density was $1.225 kg/m^3$. No-slip boundary conditions were applied to the model surfaces, which do not have any wall roughness. The free stream velocity was varied by adjusting the angle of attack during different simulation runs. The simulation was initialized uniformly with the free stream velocity throughout the entire domain. Constant fluid properties, including density and dynamic viscosity, were assumed for the prevailing incompressible flow, as there are no significant temperature changes. A convergence criterion of 10^{-5} was established for the residuals.

A grid independence study (GIS) was conducted to ensure the accuracy and reliability of the simulation. The purpose of the GIS is to determine the minimum mesh resolution required to achieve accurate results. In this study, the model from Set A was simulated using four different mesh densities: coarse, medium, fine, and extra fine. The output results for the lift coefficient were recorded, as shown in Table 2. The results indicate that the lift coefficient, C₁ value, begins to stabilize with medium meshing, so 133197 mesh nodes are acceptable.

Mesh Density	No. of Elements	No. of Nodes	Lift Coefficient, C ₁
Coarse	94717	95288	0.1956532
Medium	132537	133197	0.22286418
Fine	293608	294598	0.22224573
Extra Fine	518588	519895	0.22323133

Table 2: GIS Parameters

2.3 Solver (Processing)

For an incompressible, steady-state flow over a multiple-element airfoil, a pressure-based solver using the SIMPLE algorithm and the SA turbulence model was employed to compute the solution across the mesh. After establishing the boundary conditions and the solver, the number of iterations was specified. The number of iterations was set to 1000; however, this may change depending on the specific case, as the inlet velocity conditions vary with the angle of attack.

3.0 RESULTS AND DISCUSSION

3.1 Aerodynamics performance

Figure 4 shows the validation of this study involved by comparing the trend of the lift coefficient of the NACA 2412 airfoil with the previous study results of Ghulam et al. [15] and the data from NASA NACA series [14]. Although the Reynolds numbers differ, all models exhibit the same trend: a linear increase in the lift coefficient up to the stall angle. Beyond the stall angle $\sim 16^{\circ}$, all models show a decrease in lift.

Figure 5 illustrates the lift coefficient ($C_l \sim 0.3$ to 1.75) on the angle of attack (α) for three sets of airfoil configurations. All configurations exhibit a linear increase in C_L up to the stall angle, with slight variations among them. Set A, which combines the cambered NACA 2412 with the symmetric NACA 0012, produces moderate lift due to the limited contribution of the symmetric airfoil. The maximum lift coefficient ($C_{l,max}$) for Set A is 1.5 at $\alpha_{stall} = 14^{\circ}$. In contrast, Set B demonstrates better performance. The increased camber enhances lift generation and delays flow separation, resulting in a maximum lift coefficient ($C_{l,max}$) of 1.7 at $\alpha_{stall} = 16^{\circ}$. Set C also generates good lift but experiences an earlier stall due to the Clark Y airfoil's less efficient pressure distribution at higher angles of attack, with a maximum lift coefficient ($C_{l,max}$) of 1.65 at $\alpha_{stall} = 13^{\circ}$. Overall, the results indicate that the differences in lift coefficients among the three sets are relatively insignificant and can be considered negligible. Set B, in particular, demonstrates that this configuration can effectively delay the occurrence of stalls.

Figure 6 illustrates the drag coefficient ($C_d \sim 0.02$ to 0.19) versus the angle of attack (α) for various airfoil combinations. All configurations show a gradual increase in C_d as the angle of attack increases, indicating similar trends. Set A exhibits lowest drag because the combination of the NACA 2412 and the symmetric NACA 0012 generates more drag at higher angles. In contrast, Set C demonstrates the highest drag, particularly at larger angles, mainly because the Clark Y airfoil causes early flow separation due to its flatter bottom design. Set C reaches its peak C_d near $\alpha = 19^\circ$, highlighting significantly increased drag at steep angles. This shows that Set A is the most efficient configuration for minimizing drag, especially at higher angles of attack. At lower angles, the difference in drag among the three configurations is negligible.

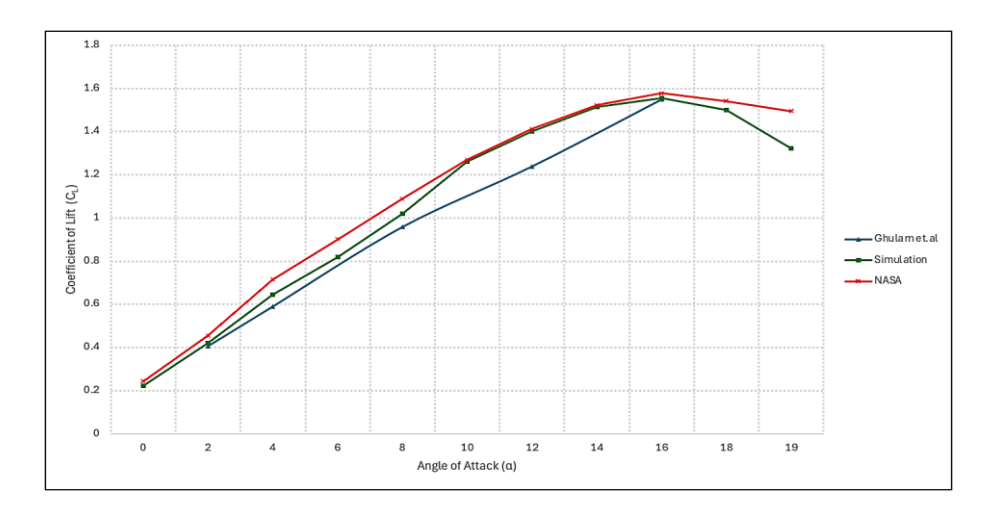


Figure 4: Lift Coefficient vs. Angles of Attack (Validation)

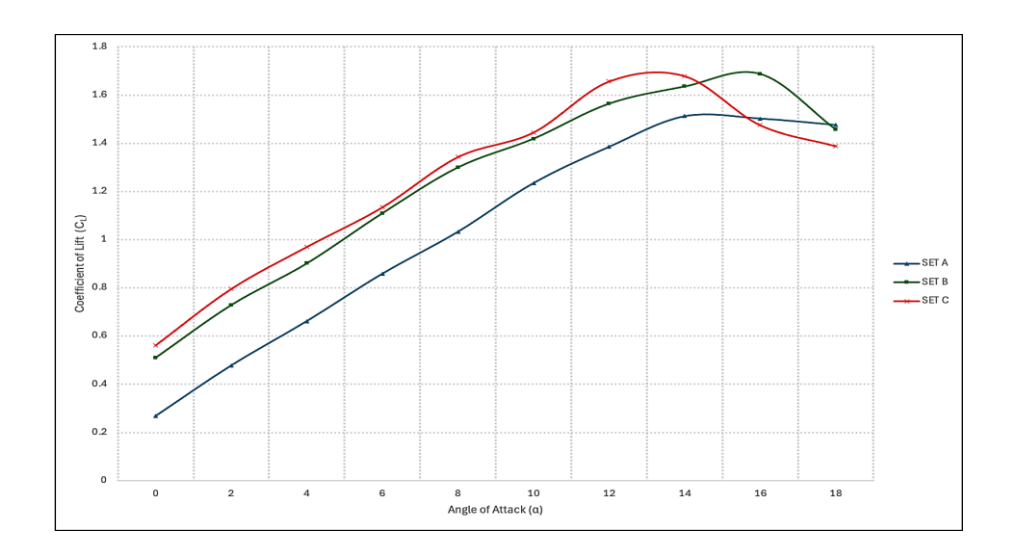


Figure 5: Lift Coefficient vs. Angles of Attack (Set A,B and C)

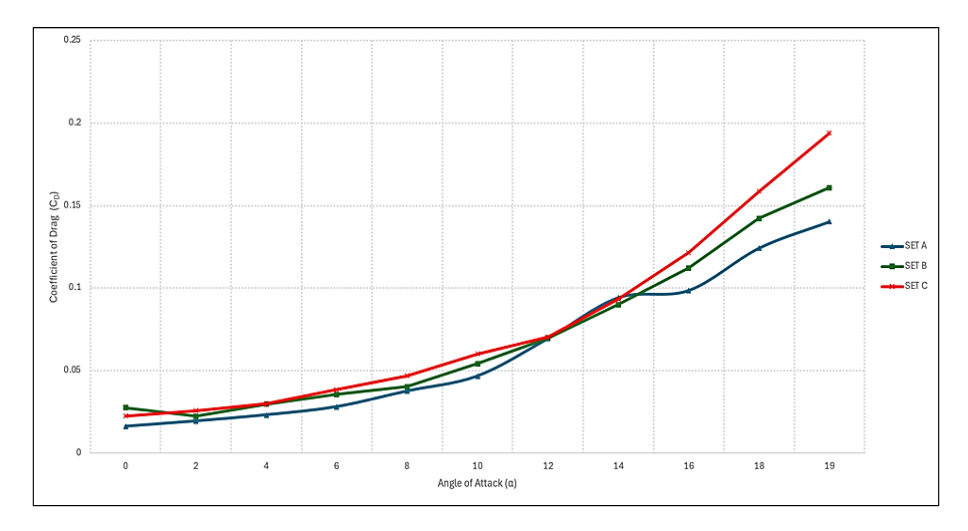


Figure 6: Drag Coefficient vs. Angles of Attack (Set A, B, and C)

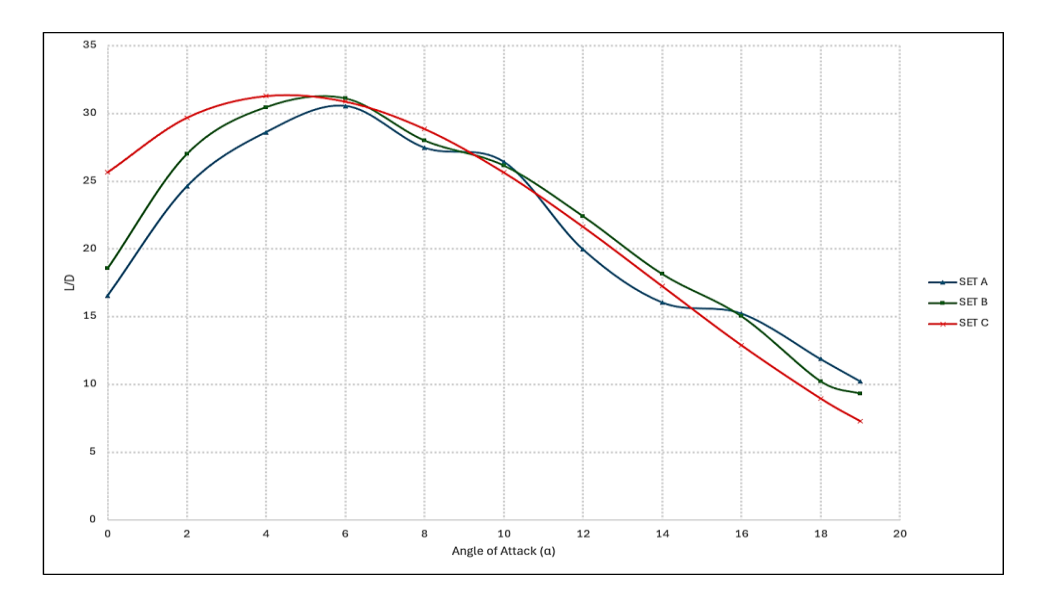


Figure 7: Lift-to-drag ratio vs. Angles of Attack (Set A, B, and C)

Figure 7 shows the lift-to-drag ratio (L/D) to the angle of attack (α) for various airfoil combinations. All combinations display an increase in L/D as the angle of attack rises, reaching a maximum L/D value at different angles before decreasing due to increased drag. The graph reveals that Sets A and B achieve a maximum L/D of approximately 32 at an angle of 5°. In contrast, configuration Set C reaches the highest L/D of around 32 at an angle of 4°. These results suggest that to achieve optimal aerodynamic performance, all configurations should operate at angles of attack where they attain their maximum lift-to-drag ratio (L/D).

3.2 Pressure contour

Figure 8 shows pressure contours for sets A, B, and C at selected angles of attack of 0°, 14°, and 18°. A crucial concept in aerodynamics is the presence of negative pressure, also known as suction, on the upper surface of the airfoil. In the context of the provided contours, where the colour bar indicates pressure relative to a reference (static pressure is shown), the negative values represent a pressure lower than the ambient free-stream pressure, which is responsible for the majority of the lift generated. The low-pressure region is created by the higher velocity of the airflow over the curved upper surface compared to the lower surface, according to Bernoulli's principle. This pressure differential (high pressure on the lower surface, negative pressure/suction on the upper surface) creates the net upward force (lift). The magnitude of the negative pressure on the upper surface is a direct indicator of the lift potential; therefore, configurations that exhibit a deeper, more extensive blue region (lower pressure) generally generate higher lift. From the results, these angles are significant: 0° represents baseline conditions, 14° indicates maximum lift at the stall angle, and 18° examines post-stall pressure behaviour. At an angle of attack (α) of 0°, the pressure distribution at the center of the airfoil reveals that the pressure on the lower surface is significantly higher than that on the upper surface. Specifically, the pressures measured are: approximately -0.146 kPa for the upper surface in set A, -86.6 kPa for set B, and -68.8 kPa for set C. In contrast, the pressures on the lower surface are around 43.7 kPa for set A, -41.0 kPa for set B, and range from -8.46 to 8.46 kPa for set C. This marked difference in pressure generates a net upward force, contributing to lift and highlighting the aerodynamic efficiency of the airfoil at this angle.

At an angle of attack (α) of 14°, the pressure distribution across the airfoil shows significant contrasts between the upper and lower surfaces. In set A, the upper surface pressure is approximately -407 kPa, while the lower surface pressure is around 239 kPa, creating a strong upward force that contributes to lift. Set B features an upper surface pressure of about -252 kPa and a lower surface pressure of -5.50 kPa, generating maximum lift just before aerodynamic stall. In set C, the upper surface pressure drops to around -419 kPa, while the lower surface pressure rises to about 239 kPa, resulting in the highest lift before stall conditions reduce efficiency.

The pressure contour at an angle of attack (α) of 18° indicates a post-stall condition. In set A, the upper surface pressure is about 241 kPa, while the lower surface pressure is around -270 kPa, leading to reduced lift and increased drag. Set B shows a significant reversal in performance, with upper surface pressure at approximately -270 kPa and lower surface pressure at around 241 kPa, resulting in further loss of lift and heightened drag. In set C, the upper surface pressure is about -177 kPa, and the lower surface pressure is around 245 kPa, indicating continued loss of lift and increased drag typical of post-stall behaviour.

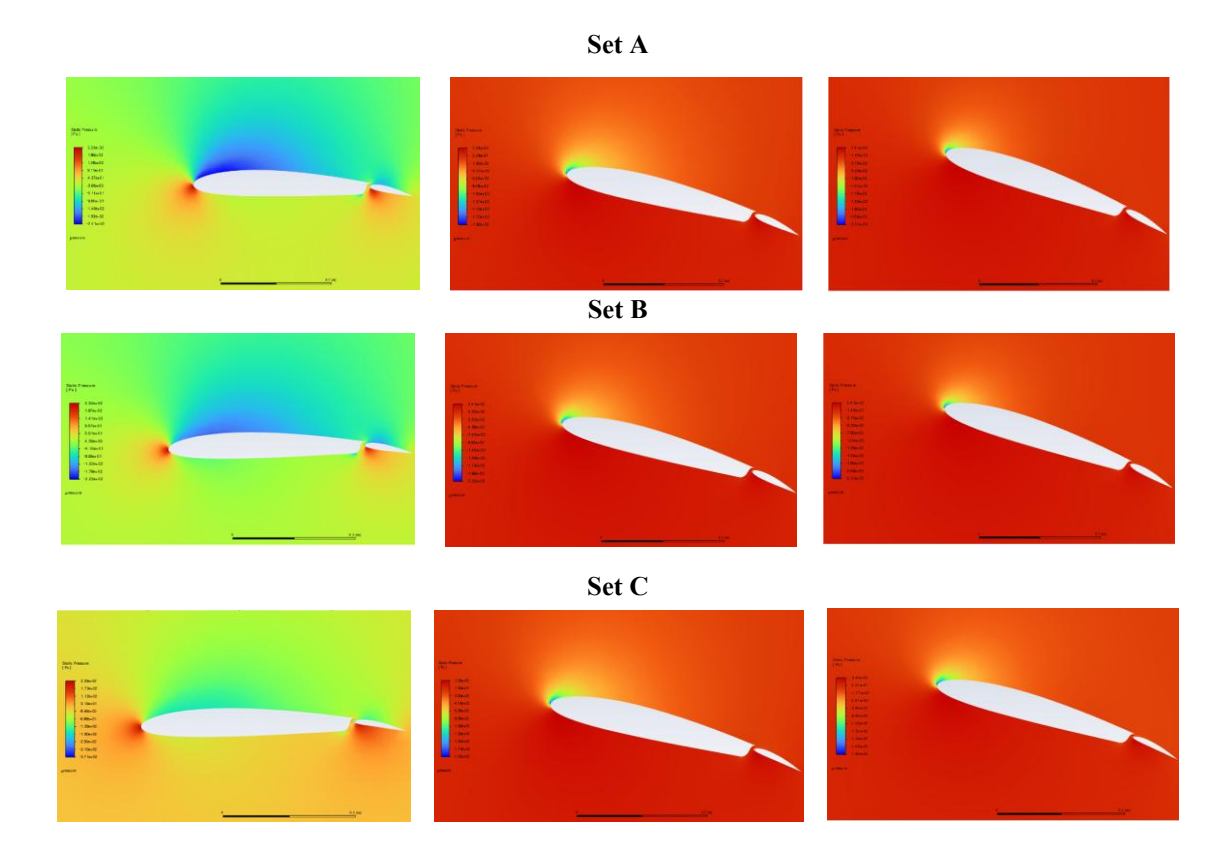


Figure 8: Pressure Contour Visualization at $\alpha = 0^{\circ};14^{\circ}$ and 18°

3.2 Velocity vectors

The velocity vector around an airfoil refers to the magnitude and direction of airflow at different points in the flow field surrounding the airfoil. It is a vector quantity, usually represented velocity in x-component (along the chord and y-component (normal to the chord). Figure 9 shows the velocity vectors for sets A, B, and C at selected angles of attack of 0° , 14° , and 18° .

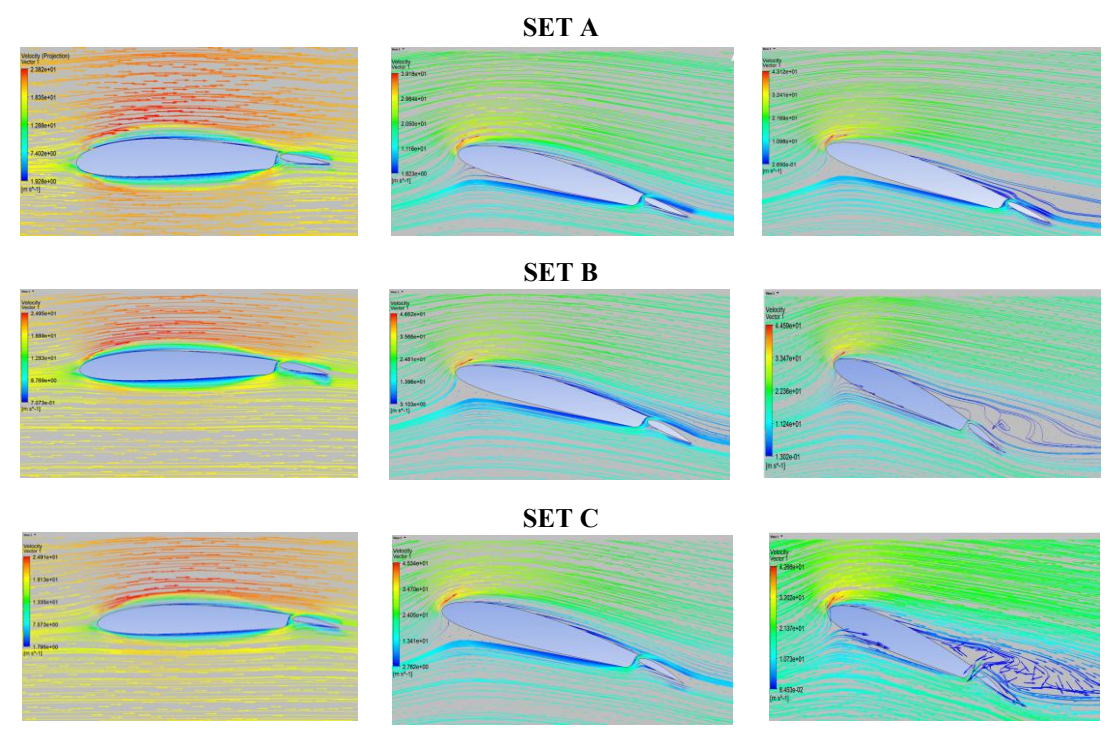


Figure 9: Velocity Vector Visualization at $\alpha = 0^{\circ};14^{\circ}$ and 18°

The velocity vector analysis for Set A at an angle of attack (α) of 0° shows smooth and attached airflow over the airfoil, which indicates efficient aerodynamic performance. The average velocity on the upper surface is 24 m/s, while the lower surface experiences a velocity of 20 m/s. This creates a pressure differential that generates lift. At this angle, the flow remains stable without any separation, ensuring optimal lift production. The attached streamlines illustrate the airfoil's ability to maintain aerodynamic efficiency at low angles of attack. As the angle of attack increases to $\alpha = 14^{\circ}$ (Set B), the airflow velocity over the upper surface peaks at 30 m/s near the leading edge but starts to separate toward the trailing edge. The lower surface velocity remains steady at 13 m/s, but the flow separation disrupts the pressure distribution. This indicates the onset of stall, at which point the airfoil reaches its maximum lift coefficient before lift begins to decline. The loss of smooth streamlines reflects reduced aerodynamic efficiency, and beyond this point, the airfoil transitions into stall. At $\alpha = 18^{\circ}$ (Set C), the airfoil enters deep stall, characterized by significant turbulence and flow separation. The upper surface velocity peaks at 43 m/s; however, severe flow separation and vortex formation dominate the trailing edge, resulting in chaotic and unsteady airflow. Meanwhile, the lower surface velocity remains at 20 m/s, but its contribution to lift is minimal due to the prevailing turbulence. The loss of attached flow leads to a sharp drop in lift and a substantial increase in drag, making the airfoil aerodynamically inefficient. This progression from attached flow to complete stall highlights the critical limits of airfoil performance in aerodynamic applications.

4.0 CONCLUSION

This study aimed to determine the aerodynamic forces, specifically the lift coefficient C_l and drag coefficient C_d , of the multiple airfoils set A, set B and set C. At an angle of attack (α) of 0° , the airflow remained attached, and the airfoil efficiently generated lift with minimal drag. The addition airfoils resulted in small but measurable improvements in C_l at this angle. At the set B critical stall angle of $\alpha = 16^{\circ}$, the airfoil equipped with demonstrated the best performance, achieving the highest lift coefficient $C_l = 1.69$.

The set B delayed the onset of stall and significantly increased lift compared to the single airfoil. In post-stall conditions, all the set especially with set B, exhibited reduced turbulence and lower drag, thereby improving aerodynamic efficiency. These findings demonstrate that all the geometry of multiple airfoils effectively enhance lift and delay stall, aligning with the study's objective. In conclusion, the objective of the study to evaluate the aerodynamic forces (C_1 and C_d) and determine the impact of additional airfoil was successfully achieved. The modifications improved the aerodynamic performance of the NACA 2412 airfoil, highlighting the effectiveness of airfoil design in optimizing lift and drag characteristics.

ACKNOWLEDGEMENT

This research would not have been possible without the support from the Faculty of Mechanical Engineering, Universiti Teknologi MARA, Shah Alam Campus. I am grateful for their belief in the significance of this study. Special thanks are also to my final year project student, Mr Fakrul Fahmi for his hard work in completing this research.

AUTHORS CONTRIBUTION

Zurriati Mohd Ali conceptualized and designed the study and provided overall supervision and critical review of the manuscript; Fakhrul Fahmi and Ahmad Fathi performed the computational simulations and experimental work; Fakhrul Fahmi carried out the data analysis and prepared the initial draft of the manuscript. Nor Afifah Yahya and Iskandar Shah Ishak contributed to the supervision, technical validation, and critical revision of the final manuscript. All authors have read and approved the final version of the manuscript.

REFERENCES

- [1] A. J. D. Al-Khafaji, G. S. Panatov, and A. S. Boldyrev, "Investigating the Effects of Multi Aerofoil Wing on the Aerodynamic Characteristics," in *5th Int. Conf. Eng. Technol. its Appl.(IICETA)*,2022, pp. 133–139, doi: 10.1109/IICETA54559.2022.9888511.
- [2] N. R. Kluga, "A Study of Flap Management, an Analysis of the Consequences of Flap Management, and a Search for Possible Causes," *J. Aviat. Educ. Res.*, vol. 1, no. 3, pp10-25 1991, doi:10.15394/jaaer.1991.1026.
- [3] H. H. Hurt Jr., Aerodynamics for Naval Aviators (rev. ed.). The Office of the Chief of Naval Operations, Aviation Training Division. NAVAIR OD-80T-80. Los Angeles, CA: University of Southern California, 1965 (Online). Available: https://www.faa.gov/sites/faa.gov/files/regulations_policies/handbooks_manuals/aviation/00-80T-80.pdf
- [4] D. Foster, H. Irwin, and B. Williams, "The Two-Dimensional Flow Around a Slotted Flap," *Aeronaut. Res. Counc. Reports Memo.* 3681, no. 3681, 1971.
- [5] S. Hariyadi, B. Juni Pitoyo, N. Pambudiyatno, Sutardi, and W. A. Widodo, "Numerical Study on Single and Multi-Element NACA 43018 Wing Airfoil with Leading-Edge Slat and Slotted Flap", *Int. J. Automot. Mech. Eng.*, vol. 21, no. 3, pp. 11652–11662, Sep. 2024, doi: 10.15282/ijame.21.3.2024.16.0899.

- [6] E. Mohammad, J. Saeed, A. Fatemeh, K. Ahmad and A. Hassan. (2025). Numerical Simulation of Wavy-Flap Airfoil Performance at Low Reynolds Number: Insights from Lift and Drag Coefficient Analysis. 10.48550/arXiv.2503.05028.
- [7] C. Velkova and M. Todorov, "Study of the Influence of a Gap Between the Wing and Slotted Flap on the Aerodynamic Characteristics of Ultra-Light Aircraft Wing Airfoil," *Rev. Air Force Acad.*, vol. 13, no. 3, 2015, pp. 39–44. doi: 10.19062/1842-9238.2015.13.3.6.
- [8] D.C. Wilcox, *Turbulence Modelling for CFD 3rd Edition*. 1993. [Online]. Available: http://www.dcwindustries.com
- [9] B. E. Launder and D. B. Spalding, "The Numerical Computation Of Turbulent Flows," *Comput. Methods Appl. Mech. Eng.*, vol. 3, no. 2, 1974, pp. 269–289.doi: 10.1016/0045-7825(74)90029-2.
- [10] L. Howarth, "Theory of Wing Sections," Physics Bulletin, vol. 11, no. 10. 1960, pp. 210–255. doi: 10.1088/0031-9112/11/10/006.
- [11] P. R. Spalart and Allmaras S.R., "A one-equation turbulence model for aerodynamic flows," *La Recherche Aerospatiale*, no. 1. 1994, pp. 5–21.
- [12] R. Allocious Britto Rajkumar; N. Mohammed Raffic; Dr. K. Ganesh Babu; V. Vignesh, "Comparative Study on Effective Turbulence Model for NACA0012 Airfoil using Spalart Allmaras as a Benchmark," *Int. J. Trend Sci. Res. Dev.*, vol. 4, no. 3, pp. 1049–1056, 2020, [Online]. Available: http://www.ijtsrd.com/papers/ijtsrd30824.pdf%0Ahttps://www.ijtsrd.com/engineering/aeronautical-engineering/30824/comparative-study-on-effective-turbulence-model-for-naca0012-airfoil-using-spalart--allmaras-as-a-benchmark/r-allocious-britto-rajkumar
- [13] S. L. Brunton, B. R. Noack, and P. Koumoutsakos, "Machine Learning for Fluid Mechanics," *Annu. Rev. Fluid Mech.*, vol. 52, pp. 477–508, 2020, doi: 10.1146/annurev-fluid-010719-060214.
- [14] "AirfoilTools." Accessed: Jan. 07, 2025. [Online]. Available: https://www.airfoiltools.com/
- [15] K. Ghulam, F. Ali, and A. A. Khan Gorar, "Optimizing the Performance of different Airfoils at Various Angles of Attack through CFD Simulation," *Int. J. Sci. Res. Sci. Eng. Technol.*, vol. 11, no. 2, pp. 23–36, 2024, doi: 10.32628/ijsrset2411145.